https://doi.org/10.5194/egusphere-2026-3129
Preprint. Discussion started: 27 July 2026

Measurement report: Seasonal Secondary and Biomass-Burning Aerosol Sources and Enhancements of Cloud Condensation Nuclei at a Central US Background Site

Maria A. Zawadowicz[1], Amie Dobracki[2], Janek Uin[1], Rebecca Trojanowski[3]

[1]Environmental Science and Technologies, Brookhaven National Laboratory, Upton, NY 11973
[2]Rainmaker Technology Corporation, El Segundo, CA 90245
[3]Interdisciplinary Science, Brookhaven National Laboratory, Upton, NY 11973

Correspondence to: Maria A. Zawadowicz (mzawadowi@bnl.gov)

Abstract.

Long-term measurements of aerosol chemistry are essential for understanding seasonal source variability and aerosol–climate interactions in continental environments. We present a multi-year (2021–2023) analysis of submicron aerosol composition at the U.S. Department of Energy Southern Great Plains (SGP) site using co-located Aerosol Chemical Speciation Monitor (ACSM), Interagency Monitoring of Protected Visual Environments (IMPROVE) network filter measurements, and supporting optical, size-distribution, and cloud condensation nuclei (CCN) observations. Organic aerosol (OA), nitrate (NO_3), ammonium (NH_4), sulfate (SO_4), and mineral dust exhibited pronounced seasonal cycles. NO_3 and NH_4 dominated winter aerosol mass, consistent with thermodynamic partitioning of ammonium nitrate (NH_4NO_3), while OA and SO_4 peaked in spring and summer, reflecting enhanced photochemistry and biogenic precursor emissions.

Positive Matrix Factorization with a rolling-window ME-2 framework resolved biomass-burning OA (BBOA), semi-volatile oxygenated OA (SVOOA), and low-volatility oxygenated OA (LVOOA). SVOOA and LVOOA together dominated annual OA mass, with strong summer maxima, while BBOA contributed episodically during fire events. We identified 168 biomass-burning episodes using BBOA spikes detected using rolling-median residual spike detection. Fire plumes increased aerosol absorption coefficient modestly but enhanced CCN number concentrations by up to a factor of four. HYSPLIT and satellite fire products indicate dominant contributions from Great Plains grassland and cropland burns, with additional forest and distant sources. These results provide a comprehensive characterization of aerosol seasonal behavior and biomass-burning impacts in the central United States, demonstrating the value of long-term, high-time-resolution mass-spectrometric observations.

1 Introduction

Atmospheric aerosols play critical roles in Earth's climate system, air quality, and human health. Their impacts depend on particle composition, size, and sources, which affect their optical properties, hygroscopicity, and ability to act as CCN (Andreae and Rosenfeld, 2008). Long-term, chemically resolved aerosol observations are essential for understanding the processes responsible for atmospheric composition, air quality, and aerosol–cloud–radiation interactions. Aerosol physical and chemical properties—including size, volatility, oxidation state, and source contributions—vary substantially across temporal scales,

https://doi.org/10.5194/egusphere-2026-3129
Preprint. Discussion started: 27 July 2026

shaping their ecological, climatic, and health impacts (Jimenez et al., 2009). Yet despite their importance, multi-year records of speciated submicron aerosol composition remain rare. Most intensive observation periods last weeks to months, and only a limited number of long-term sites worldwide provide continuous, multi-year measurements of OA and inorganic components using modern mass-spectrometric techniques (Heikkinen et al., 2020; Schmale et al., 2018; Zhang et al., 2007). As a result, understanding of seasonal and interannual variability in aerosol sources in rural, continental environments remains incomplete. In the United States (US), the SGP site offers an opportunity to address this gap. SGP is one of the world's longest-running atmospheric observatories and, due to its location in Northern Oklahoma, it is influenced by a diverse mixture of local and regional sources, including agricultural emissions, biogenic precursors, industrial pollution, and episodic biomass-burning plumes (McComiskey and Ferrare, 2016; Parworth et al., 2015; Sisterson et al., 2016). The more recent deployment of a quadrupole ACSM (Ng et al., 2011) and the IMPROVE filter network (Malm et al., 1994) provides a rich dataset of aerosol composition. While the ACSM offers high-time-resolution (30 min) speciation of non-refractory submicron aerosol, IMPROVE measurements provide robust quantification of refractory components such as mineral dust. Together, these observations enable a comprehensive assessment of seasonal aerosol behavior, source influences, and the interplay between primary and secondary components.

The first objective of this study is to characterize the seasonal and diurnal variability of inorganic and organic aerosol mass at SGP. Previous work in the central and southeastern US has shown strong seasonal cycles in SO_4 and SOA, driven by summertime photochemistry, biogenic emissions, and regional transport (Hidy et al., 2014; Kim et al., 2015; Marais et al., 2016). Likewise, wintertime accumulation of NO_3 linked to agricultural NH_3 and stable boundary layers is a well-documented regional feature (Hand et al., 2012). Our analysis of the 2021–2023 ACSM and IMPROVE records reveals pronounced seasonal gradients in NO_3, NH_4, SO_4, and OA, with distinct discrepancies between ACSM and IMPROVE organics that illuminate the role of semi-volatile species and potential filter sampling biases.

A second objective is to quantify the sources of OA at SGP using Positive Matrix Factorization (PMF) with a rolling-window implementation. Numerous aerosol mass spectrometer (AMS/ACSM) studies in rural regions have identified three robust OA source categories—biomass burning OA (BBOA), semi-volatile oxygenated OA (SVOOA), and low-volatility oxygenated OA (LVOOA)—that differ in volatility, oxidation state, and origin (Crippa et al., 2014; Ng et al., 2010; Parworth et al., 2015; Zhang et al., 2011). By applying a seasonally informed and then temporally adaptive ME-2 PMF framework (Canonaco et al., 2021a), we quantify the evolution of OA sources across seasons and years and demonstrate that SVOOA and LVOOA dominate the annual OA burden, while BBOA contributes episodically during fire events. The rolling window approach allows factor profiles to evolve smoothly over time, yielding a physically consistent interpretation of OA sources under changing meteorological and chemical regimes (Canonaco et al., 2021a).

A third objective is to assess the influence of biomass-burning emissions on aerosol composition, optical properties, and CCN activity at SGP. Biomass-burning plumes reaching the central US originate from a range of fuel types—including cropland, grassland, prescribed prairie burns, and distant forest fires—and experience significant chemical aging during transport (Cubison et al., 2011; Hodshire et al., 2019; Sedlacek et al., 2022). By using BBOA factor loadings to identify plume intercepts

https://doi.org/10.5194/egusphere-2026-3129
Preprint. Discussion started: 27 July 2026

and combining Hybrid Single Particle Lagrangian Integrated Trajectory (HYSPLIT) model back-trajectories with Global Fire Assimilation Systems (GFAS) emissions and Moderate Resolution Imaging Spectroradiometer (MODIS) land-use datasets, we determine the likely fuel categories and transport pathways influencing SGP. We further evaluate the response of absorption properties and CCN concentrations to fire plumes, providing insight into how biomass burning modifies aerosol–radiation and aerosol–cloud interactions in a region where fire impacts are less characterized than in the western US. To do this, we evaluate the CCN and optical properties of the aerosol during smoky and non-smoky periods using data from the CCN counter and optical instruments including the nephelometer and particle soot absorption spectrometer (PSAP).

Together, these analyses provide a comprehensive, multi-year perspective on the chemical drivers of aerosol variability at SGP. They illuminate the interplay between regional transport, biogenic and anthropogenic precursors, and episodic biomass-burning events in shaping OA composition and provide context for modeling studies and future field campaigns targeting the central US. The results also demonstrate the value of long-term, high-time-resolution mass-spectrometric measurements for understanding seasonal controls on aerosol sources and for constraining the representation of SOA and biomass-burning aerosol in atmospheric models.

2 Experimental

2.1 Instrumentation and Measurements

2.1.1 Aerosol Observing System (AOS)

The ARM Aerosol Observing System (AOS) (Uin et al., 2019) provided continuous measurements of aerosol size distributions, composition, optical properties, and hygroscopicity at SGP. The AOS is equipped with a 10-m collapsible inlet stack with a rain hat through which the air was sampled, and a meteorological station. Time series of select AOS measurements, such as ACSM speciated aerosol mass, number of CCN, and speciated coarse mass measured by the IMPROVE station discussed in this paper are shown in Figure 1.

2.1.2 Aerosol Chemical Speciation Monitor (ACSM)

Submicron non-refractory aerosol composition was measured with an Aerodyne (Billerica, MA) quadrupole ACSM equipped with a PM1 aerodynamic lens and a standard vaporizer. The instrument sampled from a 3 L min^{-1} flow through a PM2.5 cyclone impactor and a Nafion dryer and operated in alternating 60 s filter/sample cycles that were averaged to 28 min time resolution. The ACSM was calibrated six times over the study period. The data were corrected using a composition-dependent collection efficiency (CDCE) approach. Details of the calibration procedure, CDCE correction, and associated data processing are provided in the Supplemental Information.

https://doi.org/10.5194/egusphere-2026-3129
Preprint. Discussion started: 27 July 2026

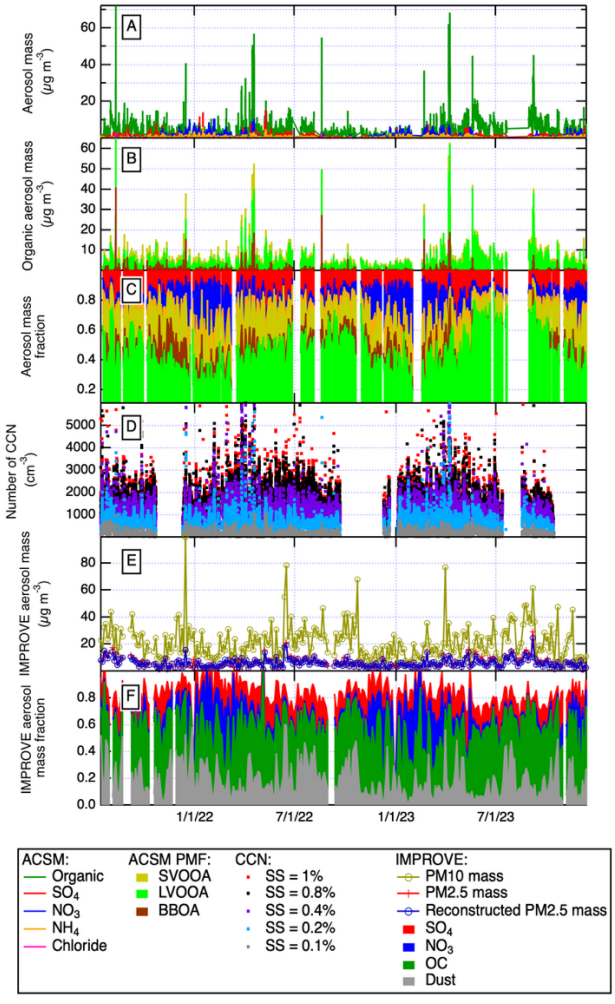

Figure 1. Summary of data used in this paper. A. ACSM speciated aerosol mass. B. Results of PMF on ACSM organic (PMF components are shown as fractions of total organic). C. Fractional aerosol species. D. Number of CCN. E. PM10 and PM2.5 from IMPROVE measurements. F. Fractional contributions from IMPROVE measurements.

2.1.3 Scanning Mobility Particle Sizer (SMPS)

A TSI (Shoreview, MN) scanning mobility particle sizer (SMPS) measured aerosol size distributions over the mobility diameter range of 10-500 nm every five minutes. The sizing accuracy of the Differential Mobility Analyzer (DMA) was verified using National Institute of Standards and Technology (NIST)-certified polystyrene latex (PSL) particle size standards (150 nm). The Condensation Particle Counter (CPC) counting efficiency was calibrated using the protocol described in

https://doi.org/10.5194/egusphere-2026-3129
Preprint. Discussion started: 27 July 2026

Hermann et al. (2007). The instrument operation was verified weekly by measuring the instrument sample flow with a bubble flow meter, and by zero tests with an HEPA filter connected to the instrument inlet.

2.1.4 Aerosol optical properties

The aerosol optical properties such as scattering and absorption coefficients, Ångstrom exponents, and single scattering albedo were calculated using a "dry" TSI nephelometer and a Radiance Research (Seattle, WA) three-wavelength particle soot absorption photometer (PSAP) deployed in the AOS (the ARM Aerosol Optical Properties (AOP) value-added product, Flynn et al., 2020). Two TSI integrating nephelometers were deployed in series with a sample RH conditioner, forming the humidigraph instrument with the first nephelometer in series designated as "dry" and the second as "wet". Both the nephelometers and the PSAP sample through and impactor assembly which periodically switches the sample between impactors with 10 μm and 1 μm cut sizes. Only dry nephelometer data without the impactor are used in this study. The nephelometers are periodically calibrated with dry CO_2 gas.

2.1.5 Cloud Condensation Nuclei (CCN)

CCN number concentrations were measured continuously at the AOS using a DMT (Longmont, CO) dual-column CCN counter and used as an indicator of aerosol cloud activation potential. The CCN counter is calibrated using size-selected ammonium sulfate at several temperature gradients. In this study, the CCN data processed to .b1-level were analyzed together with ACSM composition and SMPS size distributions to assess relationships among aerosol chemistry, size, and activation behavior.

2.1.6 IMPROVE Filter Measurements

Filter-based particulate measurements from the IMPROVE network, including PM2.5 and PM10 mass and bulk chemical composition, were used as an independent lower-time-resolution dataset. The IMPROVE filters are acquired for 24 hours every three days and analyzed for total aerosol mass, elemental mass and light absorption (Malm and Hand, 2007). These measurements complemented the higher-time-resolution AOS observations and were used to examine temporal variability in total particulate mass and broad compositional contributions over the study period. The IMPROVE-derived PM2.5 and PM10 mass concentrations and their fractional composition used in this work are shown in Figure 1.

2.2 Computational Analysis

2.2.1 Positive Matrix Factorization (PMF)

PMF (Paatero and Tapper, 1994) was applied to ACSM data using the multilinear engine (ME-2) algorithm (Paatero, 1999) with rolling PMF analysis (Canonaco et al., 2021b). Source apportionment was conducted using SoFi software (Canonaco et

https://doi.org/10.5194/egusphere-2026-3129
Preprint. Discussion started: 27 July 2026

al., 2013), with post-processing in MATLAB (2020b). The details of pre- and post-processing and of the PMF analysis are given in Supplemental Information.

2.2.2 Non-Parametric Wind Regression (NWR)

NWR (Henry et al., 2009) was applied using ZeFir software (Petit et al., 2017) with wind speed and direction recorded at the AOS meteorological station. These regressions were combined with aerosol measurements to assess source influences.

2.2.3 HYSPLIT Back-Trajectory Analysis

Hourly 7-day back-trajectories terminating at the SGP site (10 m AGL) were calculated using the NOAA HYSPLIT model (Stein et al., 2015) with NCEP/NCAR reanalysis meteorology. Concentration-weighted trajectory (CWT) analysis (Fleming et al., 2012) was implemented in ZeFir (Petit et al., 2017) to identify source regions of observed pollutants. For the analysis of tracking biomass burning emissions, the HYSPLIT model was used in Lagrangian particle dispersion mode with 5-day backward particle dispersion runs terminating at the SGP site (10 m). The particles were assumed to be 300 nm with 1.5 g cm^{-3} density and shape factor of 1. The model assumed dry deposition but no wet deposition.

2.2.4 Modern-Era Retrospective Analysis for Research and Applications, Version 2 (MERRA-2)

Hourly (for all days of this study) and monthly (for 2020-2024) average MERRA-2 re-analysis files for surface dust mass concentration, surface OA mass concentration, planetary boundary layer height (PBLH), and 10 m wind direction were retrieved from NASA Goddard Earth Sciences Data and Information Services Center. A box centered on SGP was used, with latitude between 34.5 and 38.5, and longitude between -93.75 and -100.625.

3 Results

3.1 Seasonal Trends in Organic and Inorganic Aerosol Mass at SGP

Inorganic and organic mass loadings measured by the ACSM and the IMPROVE program show strong seasonality (Figures 1-3). Inorganic components, NO_3 and NH_4 dominate in the winter (December – February) and organic components dominate in the spring (March – May) and summer (June – August). SO_4 overall tends to trend together with the organics, with peaks in the spring and summer. This annual cycle is consistent with photochemical production of SOA both locally at the site and regionally as a result of spring and summertime biogenic volatile organic compounds (VOC) emissions (Guenther et al., 2012; Shrivastava et al., 2017) and with thermodynamic partitioning of NH_4NO_3 under cold, humid conditions in the winter (Fountoukis and Nenes, 2007; Kim et al., 2014). A similar annual cycle is measured by both the ACSM and the IMPROVE program, with high correlations between ACSM NO_3 and IMPROVE NO_3 and ACSM SO_4 and IMPROVE SO_4 on monthly basis (Pearson R^2 = 0.98 and 0.79, respectively). The correlation is not as strong between ACSM organic and IMPROVE OC

https://doi.org/10.5194/egusphere-2026-3129
Preprint. Discussion started: 27 July 2026

(Pearson $R^2 = 0.61$). Specifically, the springtime organic peak detected by the ACSM is not as well-defined in the IMPROVE measurements. Because the IMPROVE program measures aerosol mass collected on filters, it is expected to underestimate highly volatile organic components (Subramanian et al., 2004; Turpin et al., 1994), which may be consistent with more recently produced SOA in the spring.

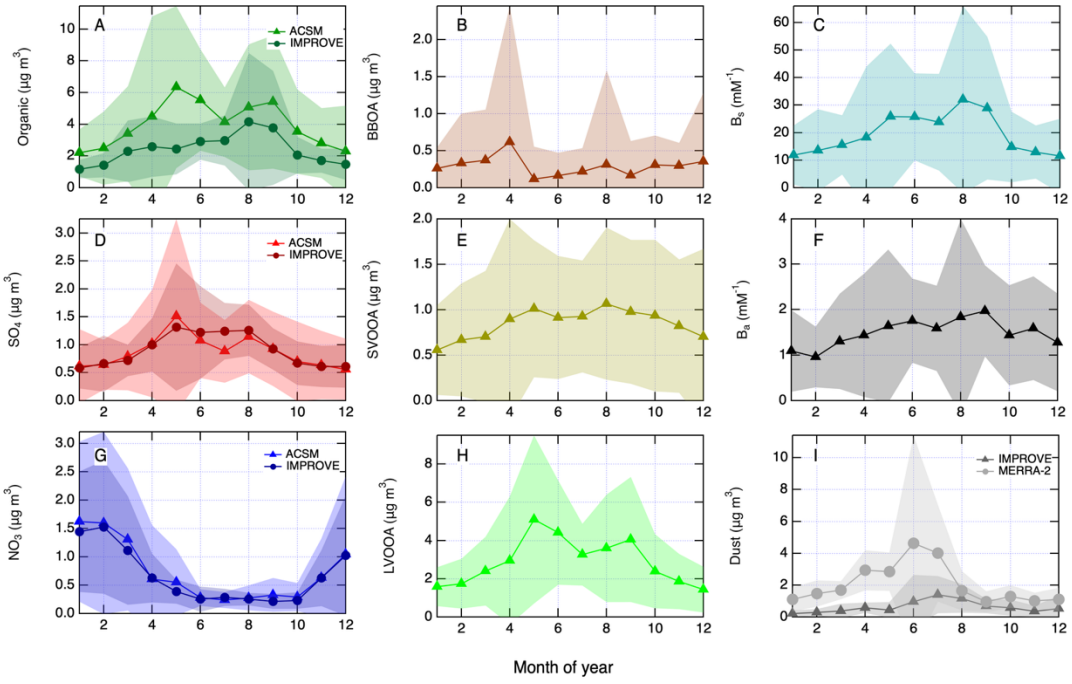

Figure 2. Annual trends in aerosol composition at SGP during 2021-2023 for various chemical components: A. ACSM and IMPROVE OA mass and OC, B. BBOA derived from PMF analysis of ACSM organic mass spectra, C. Nephelometer scattering coefficient (green), D. ACSM and IMPROVE SO_4 aerosol mass, E. SVOOA derived from PMF analysis of ACSM organic mass spectra, F. PSAP absorption coefficient (green), G. ACSM and IMPROVE NO_3 aerosol mass, H. LVOOA derived from PMF analysis of ACSM organic mass spectra, I. IMPROVE and MERRA-2 dust aerosol mass. The shading represents standard deviations.

ACSM does not measure mineral dust, but the IMPROVE program measurements include crustal components such as aluminum and silicon that allow calculation of dust loading. To this end, we used the following equation (Hand, 2023):

$$Fine\ soil\ (dust) = 2.2[Al] + 2.49[Si] + 1.63[Ca] + 2.42[Fe] + 1.94[Ti]$$

The annual trend of mineral dust concentration has a distinct peak in the summer (Figure 2I), and because of this seasonality, some of the dust can be attributed to the broader seasonal pattern of the Saharan Air Layer (SAL) (Prospero et al., 2020). A similar seasonal peak appears in MERRA-2 re-analysis data for the SGP region (Figure 2I). The weak correlation ($R^2 = 0.36$) between dust concentration derived from IMPROVE measurements and MERRA-2 surface dust concentration, suggests there are substantial contributions from local agricultural and soil sources from the Great Plains.

https://doi.org/10.5194/egusphere-2026-3129
Preprint. Discussion started: 27 July 2026

Seasonal diurnal cycles of aerosol components measured by the ACSM, as well as select optical properties and fractions of CCN aerosol budget, separated by the four seasons are shown in Figure 3. Components associated with local biogenic and agricultural emissions, such as organics in the spring and summer and NO_3 in the winter show a diurnal cycle with an early morning peak characteristic of the boundary layer. Components associated with regional and remote transport, such as SO_4 show a diurnal cycle that peaks in the mid-day.

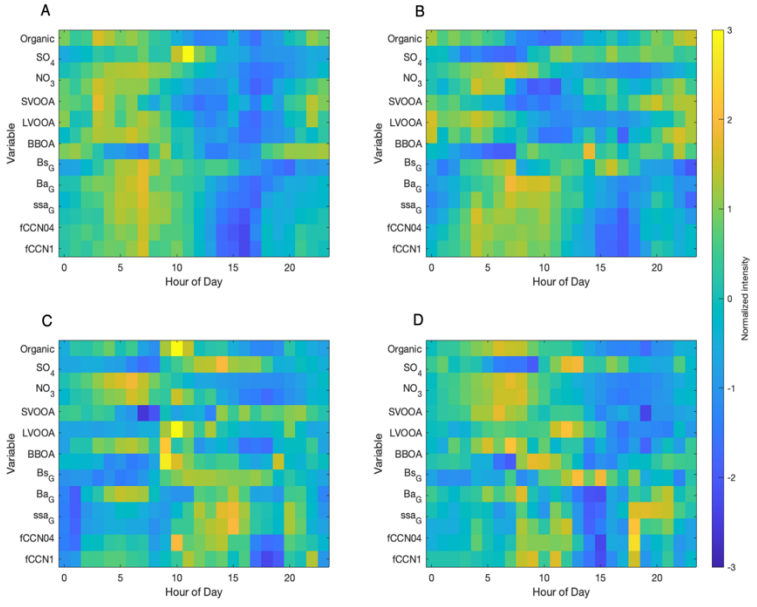

Figure 3. Diurnal cycles of select aerosol properties divided by season: A. winter (December – February), B. spring (March – May), C. summer (June – July), D. autumn (September – November). The colors represent intensity normalized to the mean.

3.2 Positive Matrix Factorization of ACSM

OA sources were apportioned using a rolling-window PMF analysis of the ACSM organic mass spectral dataset (see Supplementary Material for details). In the first step, unconstrained multilinear engine (ME-2) PMF analysis was applied seasonally, by splitting the multi-year dataset into winter (DJF, December-February), spring (MAM, March-May), summer (JJA, June-August) and autumn (SON, September-November), with multiple randomly initialized PMF runs performed for each season. This analysis is performed for 3, 4 and 5 sets of solutions (Supplemental Figures S4 – S7), and informs the selection of the best set of solutions that represents each season. All seasons, except for summer contain BBOA, SVOOA and LVOOA factors, consistent with typical AMS/ACSM factor structures at rural continental sites (Ulbrich et al., 2009; Zhang et al., 2011). Summer does not contain BBOA, due to lower amount of aerosol containing f_{60}. Spectral marker distributions characterizing individual BBOA solutions are presented for the seasons in which they occur (Supplemental Figure S8).

The ME-2 algorithm was applied with a priori constraints using reference mass spectra for two expected OA source types, SVOOA and BBOA, obtained by averaging seasonal solutions (Supplemental Figure S10), while the LVOOA factor remained unconstrained. A rolling-window approach (5-day windows advancing by 1-day steps) allowed factor profiles to adapt over

https://doi.org/10.5194/egusphere-2026-3129
Preprint. Discussion started: 27 July 2026

time and capture seasonal and synoptic variability in sources and oxidation level (Canonaco et al., 2021a). Performance and uncertainty of the PMF solution were evaluated using several diagnostics (detailed in the Supplementary Material). Scaled residuals (observed minus model signal, divided by uncertainty) from the three-factor ACSM PMF model are centered near zero (Supplemental Figure S15), indicating no systematic bias in the PMF fit. Over 95% of residuals fall within ±2, well within the acceptable range (with ±3 considered a reasonable bound for good PMF fits). These diagnostics confirm that the constrained rolling PMF achieved a good fit to the data without overfitting, and that the identified factors are statistically significant and reproducible.

On average, LVOOA was the largest contributor to OA mass over the 2021–2023 period, accounting for approximately 45% of total aerosol mass, as shown in Figure 1B, which summarizes the quantitative contribution of each OA factor. SVOOA contributed roughly 15% of aerosol mass on average, and BBOA made up typically 5% of aerosol mass annually. However, these mean values mask strong temporal variability associated with meteorology and sources, as the factor contributions exhibited clear seasonal patterns (Figures 2-3). These results reflect enhanced formation of biogenic SOA in summer, given higher emissions of VOC precursors (e.g. from vegetation) and stronger photochemical activity. LVOOA has a similar seasonal pattern that peaks in the summer (Figure 2). BBOA showed the most episodic behavior: it was low for much of the year but spiked during intermittent biomass burning events. In particular, during the spring (March–April) of each year, BBOA fractions increased, potentially due to prescribed agricultural burns in the region. These fire influenced periods are analyzed further in Sect. 3.3.

Seasonally-resolved correlations among aerosol components and factors provide additional insight into source relationships (Figure 4). The PMF factor time series were compared with external tracers and with each other to verify that they represent distinct sources. We find that the LVOOA factor correlates moderately with SO_4 (with a Pearson R^2 = 0.3-0.4 across the full dataset), consistent with a regionally transported secondary aerosol influence, as SO_4 and highly aged organics often accumulate together in broad regional haze. NO_3 is generally correlated with NH_4 (R^2 = 0.87 in the winter), confirming that it exists predominantly as NH_4NO_3, especially during winter episodes of high NO_3. The two oxygenated OA factors (LVOOA and SVOOA) are moderately correlated with each other (R^2 ~0.3–0.6) since both respond to general OA loadings and often co-exist, though their ratio varies by season. These correlation patterns support the interpretation of the PMF factors: LVOOA as regionally transported aged aerosol, SVOOA as local/semivolatile secondary OA, and BBOA as isolated biomass burning contributions. They are also consistent with prior AMS/ACSM source apportionment studies, which universally find one or two oxidized OA factors dominating rural aerosol and a separate BBOA factor during fire impacts.

https://doi.org/10.5194/egusphere-2026-3129
Preprint. Discussion started: 27 July 2026

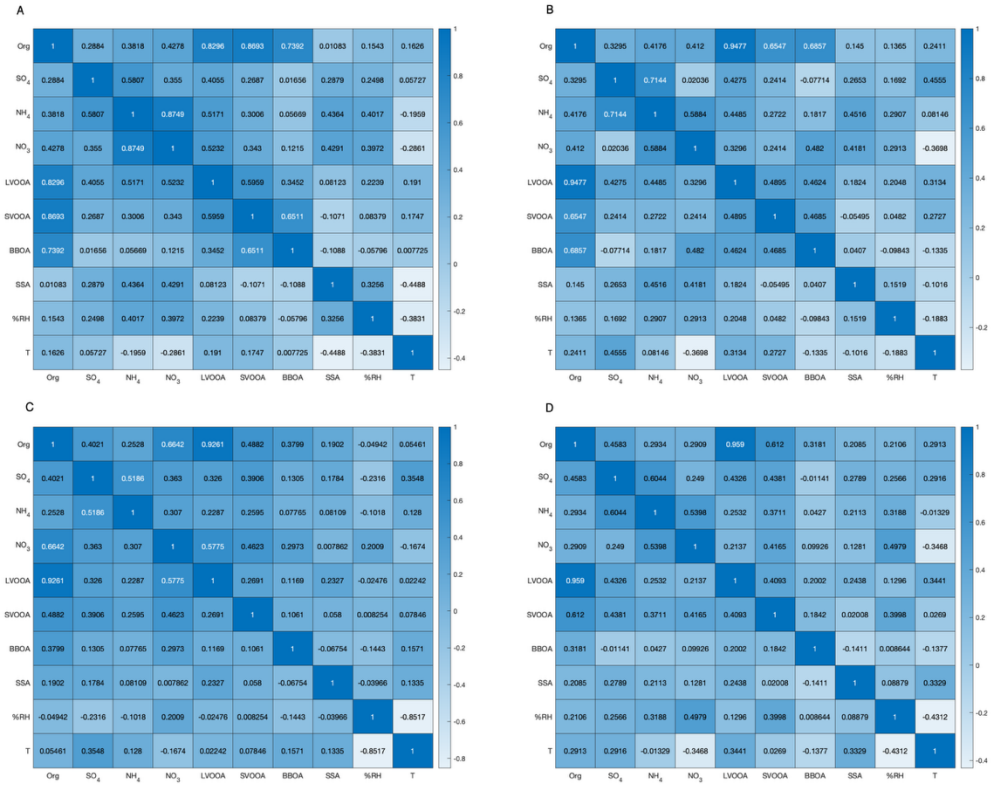

Figure 4. Pearson correlations of select aerosol and environmental properties divided by season: A. winter (DJF), B. spring (MAM), C. summer (JJA), D. autumn (SON)

3.3 Comparison of smoky and non-smoky conditions

The presence of BBOA factor was used to isolate distinct fire events from the time series of ACSM measurements. BBOA fire influences were identified as statistically significant positive anomalies relative to a time-varying local background. Specifically, a past-only 48-hour rolling median was used to define a dynamic BBOA baseline, residuals (observed – baseline) were calculated, and hours exceeding a robust threshold of 2 × IQR/1.349 (≈2σ) (where IQR – inter-quantile range) were flagged as spikes; consecutive spike hours separated by ≤3 hours were grouped into individual fire events. The temporal distribution of the 168 distinct fire events that were identified is shown in Supplemental Figure S17. There is markedly fewer BBOA events in 2023 compared to 2021-2022, which is consistent with continental US fire statistics (NOAA National Centers for Environmental Information, 2024).

Changes in aerosol optical properties during fire event windows relative to background conditions (monthly averages excluding fire periods) are shown (Figure 5). The absorption coefficient (B_a) and absorption Ångström exponent exhibit modest increases during fire events. In contrast, the scattering Ångström exponent and single scattering albedo (SSA) show little change.

https://doi.org/10.5194/egusphere-2026-3129
Preprint. Discussion started: 27 July 2026

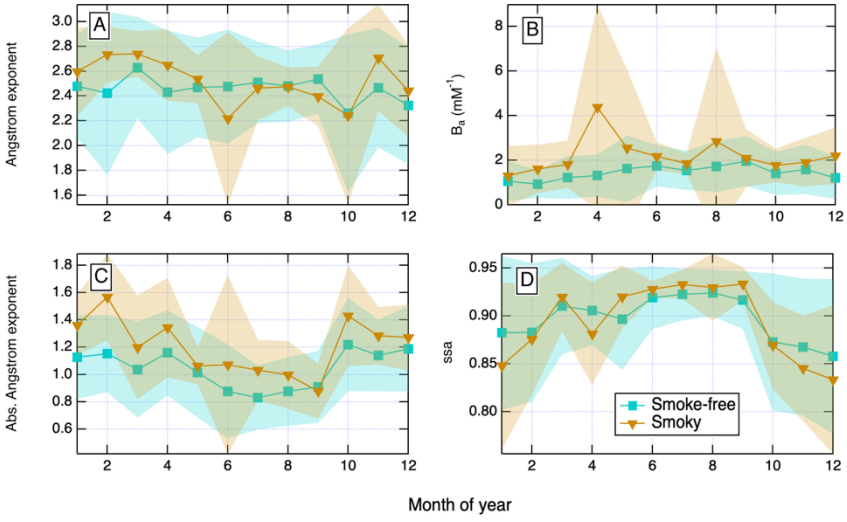

Figure 5. A comparison of aerosol optical properties during smoky and smoke-free periods at SGP across all seasons. A: Ångström exponent (blue – red wavelengths), B: Absorption (green wavelength), C: Absorption Ångström exponent (blue – red wavelengths), D: Single scattering albedo (green wavelength).

Comparisons of CCN number concentrations during fire event windows and background conditions are similarly presented (Figure 6). In this case, the fire influence is more pronounced: CCN number concentrations increase by as much as a factor of four during spring fire events relative to background conditions. However, this increase is not reflected in the CCN fraction (N_{CCN}/N_{CN}; Supplemental Figure S16), suggesting that the BBOA particles themselves are not strongly hygroscopic. Instead, the increase in particle number concentration (and potentially particle size) during fire events likely drives the greater availability of CCN.

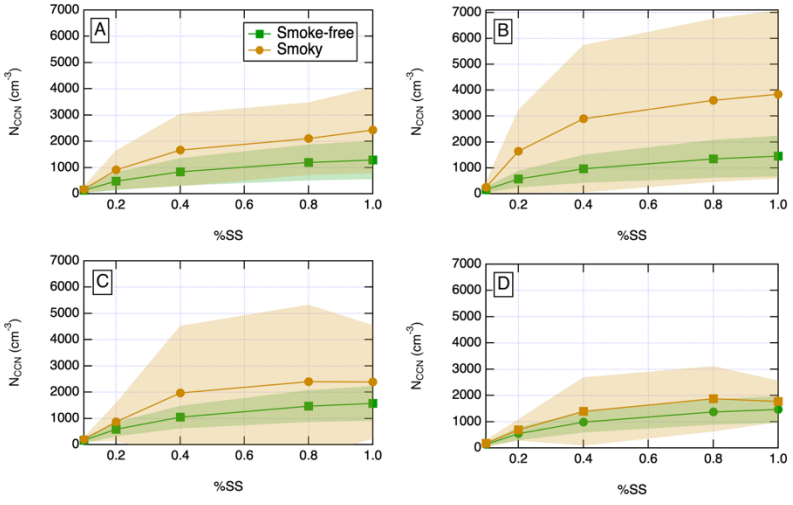

Figure 6. A comparison of number of CCN at different supersaturations during smoky and smoke-free periods at SGP split by season. A: DJF, B: MAM, C: JJA, D: SON.

https://doi.org/10.5194/egusphere-2026-3129
Preprint. Discussion started: 27 July 2026

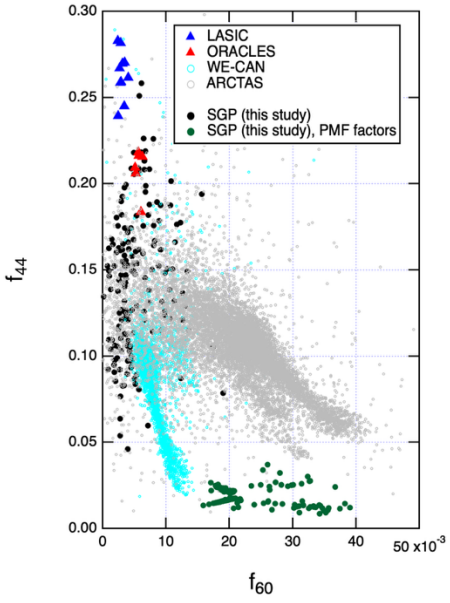

Figure 7. A comparison of f_{44} vs f_{60} spectral markers from the fire events analyzed in this study to measurements from LASIC, ORACLES, WE-CAN and ARCTAS campaigns.

The lack of clear optical signature of the biomass burning events suggests that the BBOA plumes observed at SGP are significantly aged. Here we compare SGP f_{44} and f_{60} markers to those observed during 2016-2017 Layered Atlantic Smoke Interactions with Clouds (LASIC) (Dobracki et al., 2025), 2016 ObseRvations of Aerosols above CLouds and their intEractionS (ORACLES) (Dobracki et al., 2023), 2018 Western wildfire Experiment for Cloud chemistry, Aerosol absorption and Nitrogen (WE-CAN) (Twohy et al., 2021) and 2008 Arctic Research of the Composition of the Troposphere from Aircraft and Satellites (ARCTAS) (Jacob et al., 2010) campaigns (Figure 7). SGP fire plumes have a broad distribution of f_{44} and f_{60}, consistent with emissions of variable photochemical ages, but they tend to be more processed than the BBOA emissions observed during WE-CAN and ARCTAS and less processed than the emissions observed during ORACLES and LASIC. This pattern is consistent with measurements at a continental receptor site influenced by fires from the same continent, without additional processing in the marine boundary layer. The f_{44} and f_{60} distributions of the PMF factors isolated from the rolling PMF windows associated with the BBOA events are also shown in Figure 7 (green markers). These factors exhibit signatures of fresh BBOA, characterized by high f_{60} and low f_{44}, and thus more directly represent source-emission profiles.

4 Discussion

4.1 Source apportionment of inorganic aerosol components

Elevated SO_4 concentrations occur under higher wind speeds across all seasons (Figure 8a–d), indicating that SO_4 at the site is primarily influenced by regional transport rather than local emissions or recirculation. The directional patterns further

https://doi.org/10.5194/egusphere-2026-3129
Preprint. Discussion started: 27 July 2026

reinforce this interpretation: the strongest enhancements are associated with southerly winds. Such behavior is consistent with the advection of aged, regionally processed aerosol from upwind urban, industrial, and maritime regions, where precursor gases (e.g., SO_2) undergo oxidation during transport before arriving at the site.

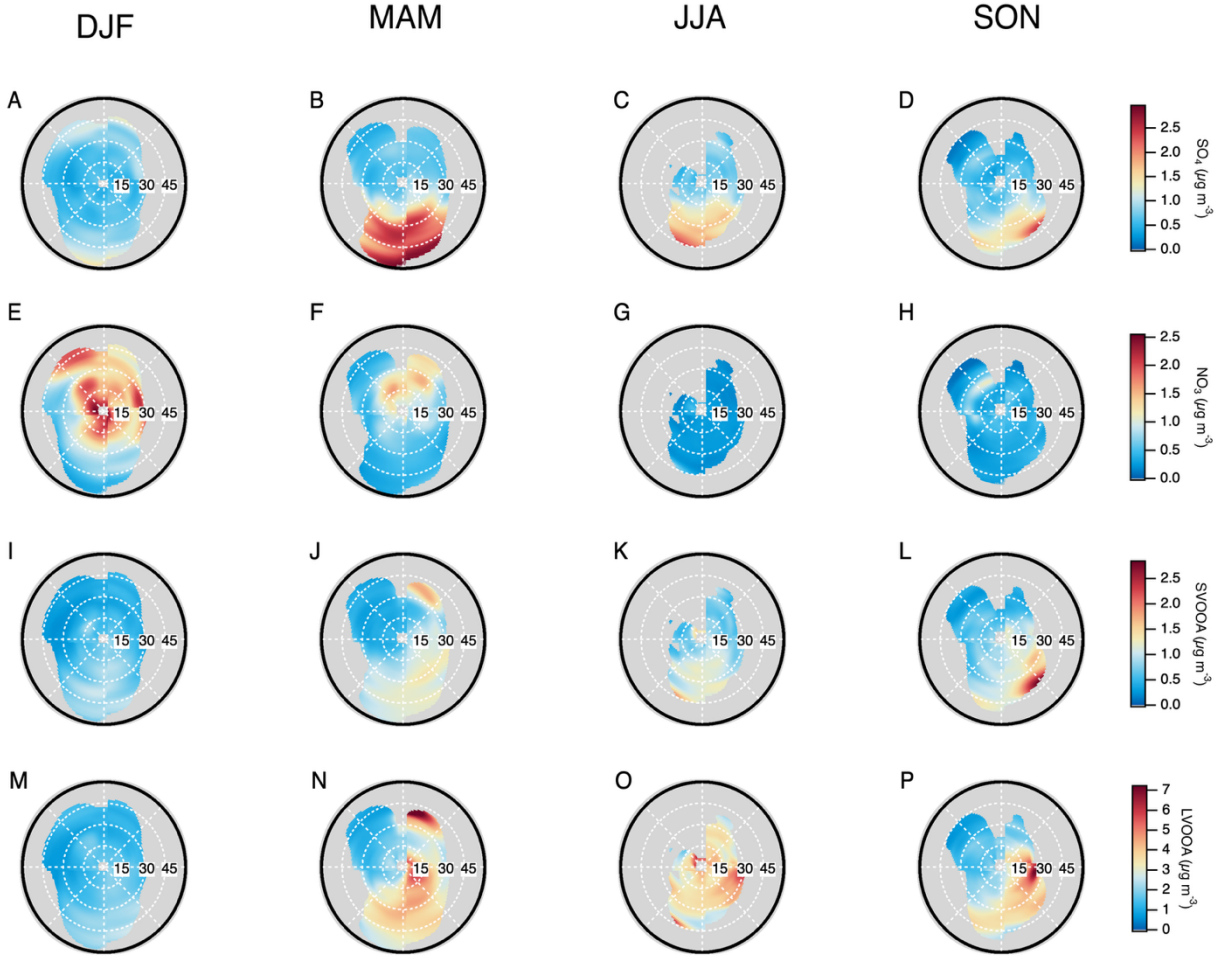

Figure 8. Non-parametric wind regression for inorganic and organic aerosol mass at SGP.

In contrast, NWR analysis for NO_3 (Figure 8e–h) reveals a substantially weaker dependence on wind speed, suggesting a superposition of both local and regional contributions. The directional signal for NO_3 is more spatially confined and predominantly oriented toward the northeast. This pattern indicates that nearby continental sources—including agricultural NH_3 emissions, local combustion plumes, and episodic regional transport—likely modulate the observed NO_3 variability. The reduced wind-speed sensitivity and sharper directional gradient for NO_3 are consistent with its formation via thermodynamic partitioning processes occurring closer to the site (Hand et al., 2012).

https://doi.org/10.5194/egusphere-2026-3129
Preprint. Discussion started: 27 July 2026

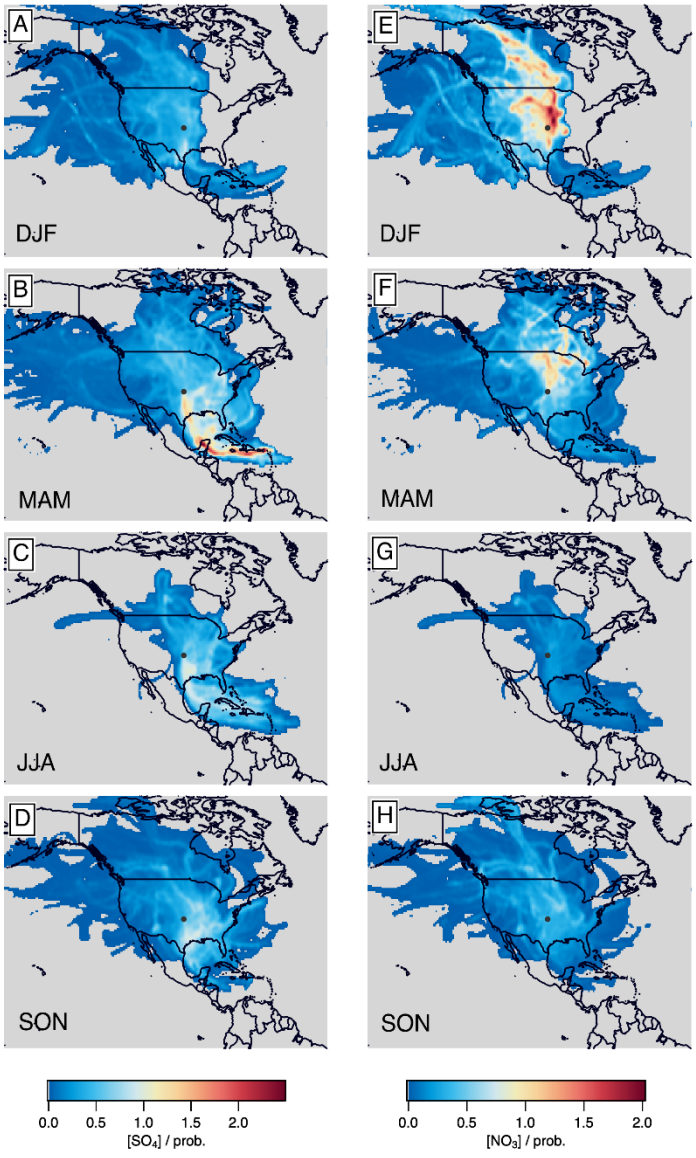

Figure 9. Concentration-weighted back-trajectory analysis for inorganic aerosol mass.

CWT analyses further contextualize these findings (Figures 10-11). For SO_4 (Figure 9), elevated CWT loadings during spring are consistently linked with air masses arriving from eastern Texas and the Gulf of Mexico. These source regions encompass
295 a mixture of urban/industrial centers, coastal petrochemical facilities, and shipping corridors, supporting the interpretation that SO_4 measured at the site predominantly reflects secondary formation during regional-scale transport (Schulze et al., 2018; Thompson et al., 2025).

The CWT patterns for NO_3 show a broader and more heterogeneous spatial footprint across the continental US, with notable contributions from upwind agricultural regions. This spatial pattern is in line with the known importance of NH_3-rich

https://doi.org/10.5194/egusphere-2026-3129
Preprint. Discussion started: 27 July 2026

agricultural emissions for NO_3 formation and further underscores the mixed local–regional origin of the observed NO_3 (Hand et al., 2012).

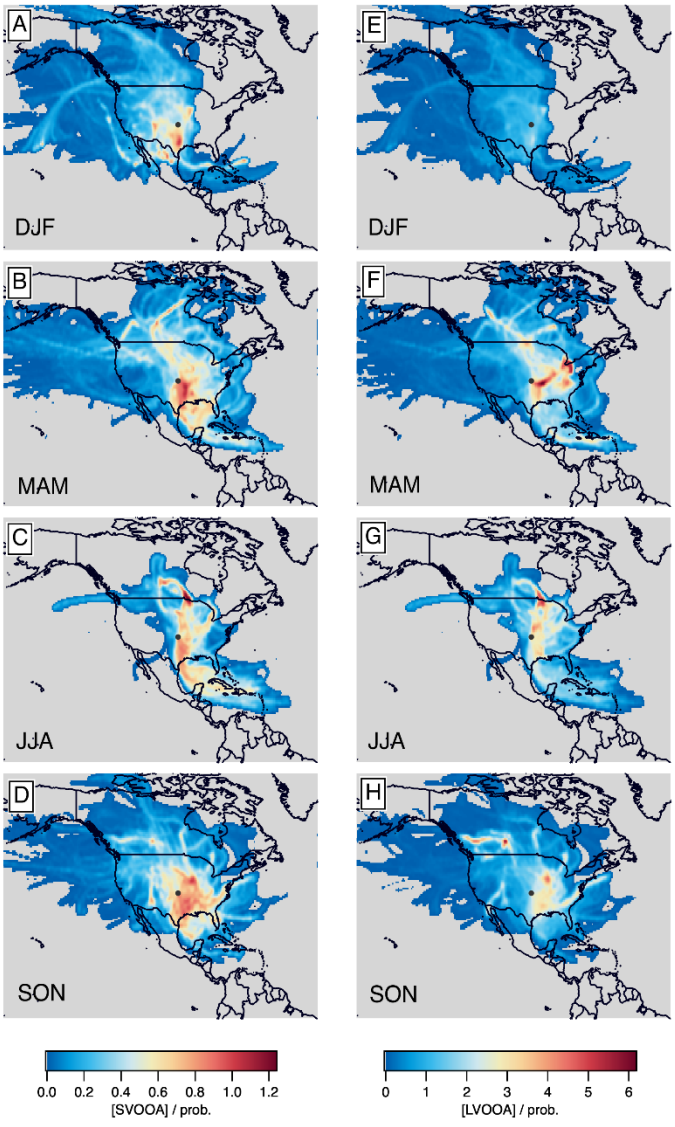

Figure 10. Concentration-weighted back-trajectory analysis for OA mass.

4.2 Source apportionment of oxidized organic components

SVOOA exhibits a broad distribution across wind speeds and directions (Figure 8i–l), indicative of both regional secondary production and contributions from nearby sources (e.g., urban emissions, biogenic precursors, and small-scale combustion). Notably, enhancements are more frequently associated with south-easterly flow, a pattern consistent with advection of photochemically processed OA from mixed urban–biogenic and agricultural source regions upwind of the site.

https://doi.org/10.5194/egusphere-2026-3129
Preprint. Discussion started: 27 July 2026

The LVOOA PMF factor (Figure 8m–p) shows a different seasonal and directional behavior. During spring and autumn, LVOOA concentrations are highest under southerly flow regimes, suggesting that long-range transported, highly aged SOA dominates during these transitional seasons. In summer, by contrast, LVOOA becomes more uniformly distributed with respect to both wind speed and direction, consistent with strong regional background formation and the influence of widespread photochemistry across the central and southeastern US (Hidy et al., 2014; Kim et al., 2015; Marais et al., 2016).

The CWT analysis (Figure 10) provides additional insight into spatial source influences for both SVOOA and LVOOA. The resulting fields point to a mixture of local and regional source contributions across the continental United States, reflecting the complexity of SOA formation pathways. SVOOA exhibits somewhat more localized potential source regions, whereas LVOOA shows broader continental-scale influence patterns consistent with extensive atmospheric aging. Seven-day HYSPLIT back trajectories were combined with dominant MODIS land-use categories along the trajectory paths to provide a land-use–specific view of aerosol composition (Figure 11). When air masses are categorized as forest-dominated (≥50% of back-trajectory of residence time in any of the MODIS forest land-use categories), both SVOOA and LVOOA exhibit substantially higher median concentrations compared with other categories. This result highlights the importance of forested regions as sources of volatile organic compounds (VOCs), such as terpenes, that ultimately contribute to SOA formation. However, forest-dominated air masses are relatively rare in this dataset (n = 38), limiting the statistical robustness of this interpretation, although the signal is consistent with well-established biogenic SOA formation mechanisms (Shrivastava et al., 2017).

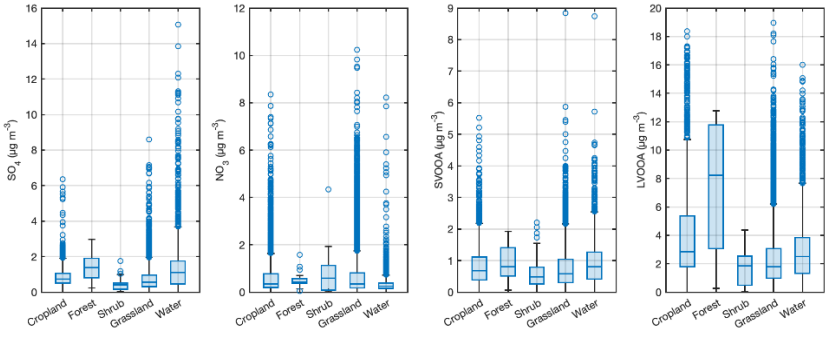

Figure 11. Means (box) and standard deviations (whiskers) for SO_4, NO_3, SVOOA and LVOOA grouped by dominant MODIS land-use categories co-incident with HYSPLIT back-trajectories.

4.3 Source apportionment of biomass burning aerosol

The episodic nature of BBOA requires a source-apportionment strategy tailored to short-lived plumes. The NOAA HYSPLIT model run in particle-dispersion mode (Stein et al., 2015) was used to generate receptor footprints for each BBOA event at SGP and identify contributing fires and their likely sources.These footprints were intersected with the CAMS GFAS $PM_{2.5}$ flux product (Kaiser et al., 2012), which is derived from satellite fire radiative power (FRP), to isolate fires whose emissions were transported to the receptor site.

https://doi.org/10.5194/egusphere-2026-3129
Preprint. Discussion started: 27 July 2026

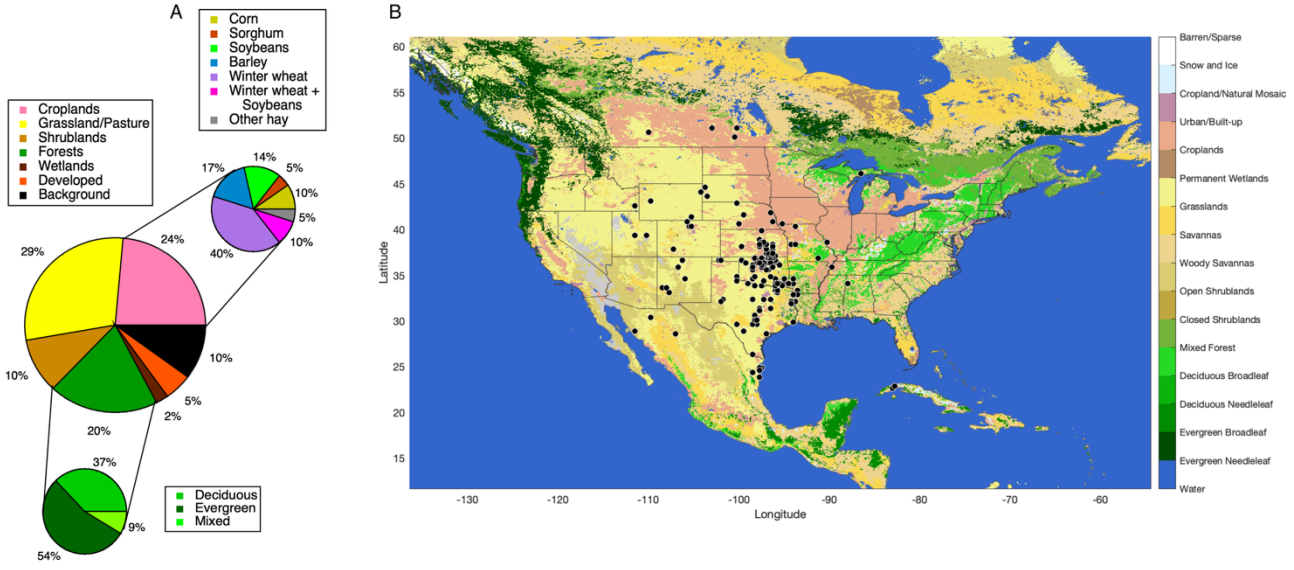

Figure 12. Likely sources for BBOA observed at the SGP site in 2021-2023. A. Inferred fuel sources for the BBOA observed at SGP (using USDA Cropland Data Layer). B. Fire locations overlaid on MODIS land use categories.

Fire coordinates are mapped onto the USDA Cropland Data Layer (Boryan et al., 2011), indicating that ~25% of source fires occurred in cultivated areas dominated by winter wheat (40–50%), with soybeans (14%) and barley (17%) as additional contributors (Figure 12). Grassland/pasture fires represent roughly 30%, and 20% originated in forested areas, primarily evergreen (54%). The spatial distribution (Fig. 12B) shows that most fires influencing SGP occurred within the Great Plains, consistent with the predominance of grassland/pasture fuel types. A smaller number of plumes were associated with fires in Canada, Mexico, or the Caribbean (Cuba).

Statistical summaries of plume characteristics separated by fuel type are presented (Figure 13). Grassland fires, which tend to occur geographically closer to SGP, produce the highest observed organic and BBOA mass loadings. In contrast, shrubland and forest plumes exhibit indicators of more extensive atmospheric processing: reduced f_{60} (Alfarra et al., 2007; Cubison et al., 2011) and enhanced SO_4, consistent with longer transport times and increased oxidation (Hodshire et al., 2019; Jolleys et al., 2015). Despite these compositional differences, the absorption coefficient, absorption Ångström exponent, and single-scattering albedo for grassland fires do not differ substantially from those for cropland or forest fires. Urban fires, though relatively infrequent, exhibit low BBOA and low f_{60}, consistent with limited vegetative fuel.

https://doi.org/10.5194/egusphere-2026-3129
Preprint. Discussion started: 27 July 2026

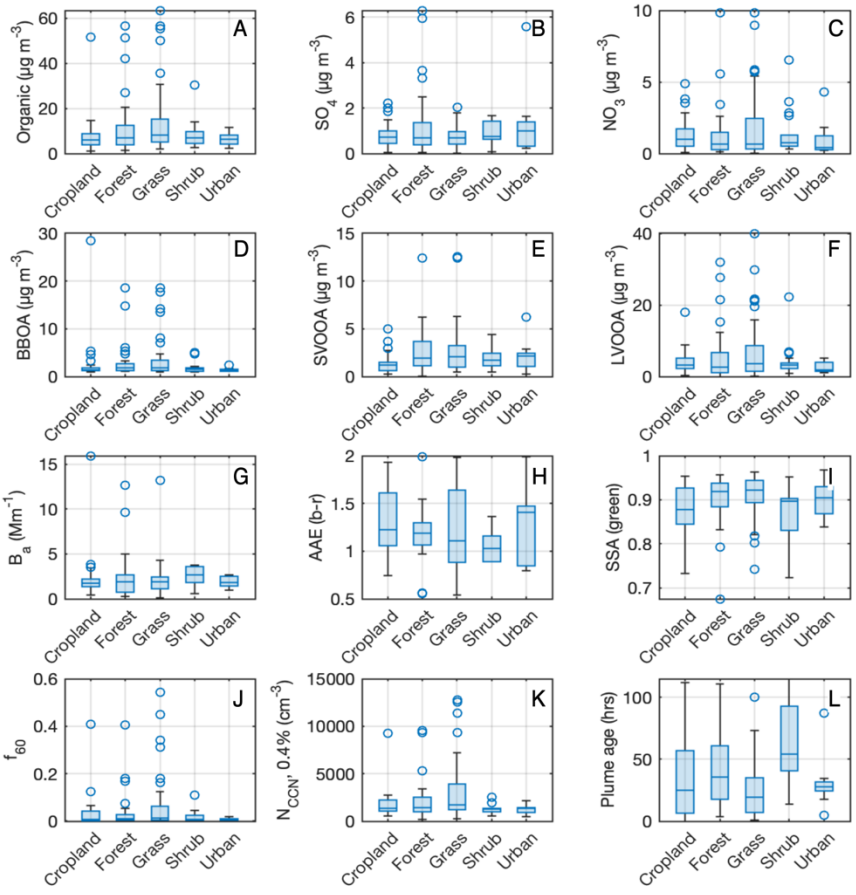

Figure 13. Mean aerosol properties associated with fuel types, as defined in Figure 11.

BBOA factor spectra derived from PMF windows coincident with plume intercepts show the distribution of f_{60} and f_{73}, colored by inferred fuel type (Figure 14a). Urban plumes display the lowest f_{60} and f_{73} values, whereas cropland, grassland, and forest plumes occupy a broader and higher-intensity range. These spectral markers reflect a combination of intrinsic fuel composition—more woody fuels contain higher levels of these fragments and of chemical processing and depositional losses during atmospheric transport, both of which are known to reduce levoglucosan-related signals (Hennigan et al., 2010; May et al., 2012).

A classification scheme for local versus regional transport was developed to account for the strong dependence of plume aging and removal processes on synoptic conditions (see Supplemental Materials for details).This scheme used correlations between ACSM organic mass and MERRA-2 reanalysis organic mass, planetary boundary layer height (PBLH), local wind speed, and

https://doi.org/10.5194/egusphere-2026-3129
Preprint. Discussion started: 27 July 2026

angular differences between local and MERRA-2 wind direction (Supplemental Figure S18). Distributions of OA and BBOA mass as a function of the plume age inferred from the HYSPLIT analysis are shown in Figure 14C and 14E prior to removing events associated with local, unfavorable transport conditions. After restricting the analysis to regional transport (Figures 15D and 15F), a clearer and physically consistent pattern emerges: younger plumes exhibit higher organic and BBOA mass, consistent with the expected decay of primary biomass-burning signatures through oxidation, dilution, and deposition (Cubison et al., 2011; Ortega et al., 2013). The relationship between f_{60} and f_{73} for regional-only plumes (Fig. 14b) remains broadly consistent with the full dataset, but with reduced scatter due to the removal of poorly constrained transport cases.

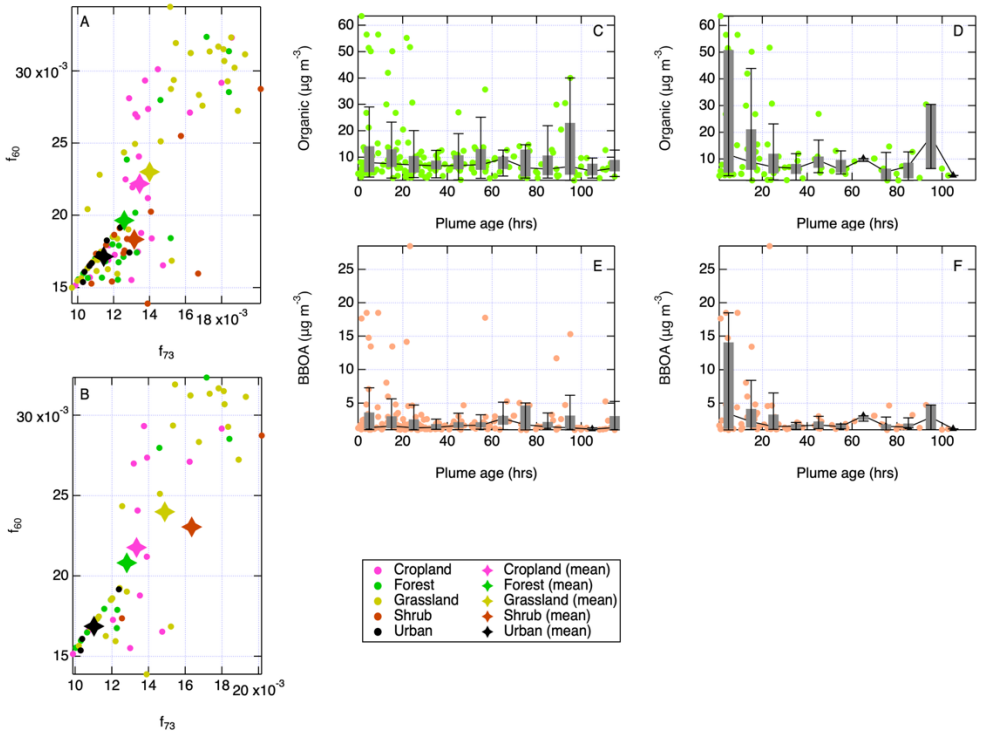

Figure 14. A. Distribution of BBOA-specific markers for various source fuel types (all BBOA plumes). B. Distribution of BBOA-specific markers for various source fuel types (BBOA plumes defined as regional only, see text). C. Peak plume organic mass vs. inferred plume age (all BBOA plumes). D. Peak plume organic mass vs. inferred plume age (BBOA plumes defined as regional only, see text). E. Peak BBOA mass vs. inferred plume age (all BBOA plumes). F. Peak BBOA mass vs. inferred plume age (BBOA plumes defined as regional only, see text).

5 Conclusion

This study provides a three year record of chemically resolved submicron aerosol composition and sources at the ARM SGP site, a rural continental environment influenced by agricultural activity, biogenic emissions, regional transport, and episodic biomass burning. Wintertime aerosol mass is dominated by NH_4NO_3, reflecting cold-season thermodynamic partitioning and regional NH_3 availability, whereas spring and summer are characterized by enhanced OA and SO_4 associated with

https://doi.org/10.5194/egusphere-2026-3129
Preprint. Discussion started: 27 July 2026

photochemical production and biogenic precursor emissions. Comparisons between ACSM OA and IMPROVE OC highlight systematic differences during spring, consistent with contributions from semi-volatile SOA that are not fully retained in filter-based measurements. Mineral dust peaks in summer and reflects a mixture of regional transport and local soil and agricultural sources. Rolling-window ME-2 analysis further demonstrates that OA is dominated year-round by oxygenated components. SVOOA and LVOOA together constitute the majority of OA mass, with strong summer maxima, confirming the importance of secondary formation pathways in this region. BBOA is highly episodic but can represent a substantial fraction of OA during fire periods. Wind-regression and trajectory analyses show that SO_4 and LVOOA are primarily associated with regional southerly transport, whereas NO_3 and SVOOA reflect mixed local–regional influences.

A total of 168 biomass-burning events were identified. Although fire plumes produced only modest average changes in bulk optical properties, they substantially increased CCN number concentrations, by up to a factor of four during spring, primarily through increases in particle number rather than intrinsic hygroscopicity. Fire source attribution indicates dominant contributions from Great Plains grassland and cropland burns, with additional influence from forest and more distant fires. Plume aging analyses show decreasing BBOA mass and spectral markers with transport time, consistent with oxidation, dilution, and depositional loss.

These seasonal patterns are broadly consistent with previous observations of winter nitrate and oxygenated OA dominance at rural continental sites (Crippa et al., 2014; Hand et al., 2012; Parworth et al., 2015; Stanier et al., 2012), while the combined source-resolved, optical, and CCN measurements provide new evidence that regional biomass burning can strongly perturb CCN abundance without producing correspondingly large changes in bulk optical properties. Interpretation of these results is nevertheless limited by the 2021–2023 record length, non-uniqueness in PMF factor resolution, sensitivity of event identification to the selected threshold, and uncertainties in trajectory calculations and satellite-based fire and fuel attribution; moreover, the observational comparison between smoky and non-smoky periods does not by itself establish a causal cloud response. Within these constraints, the results indicate that models of central-US aerosol and CCN variability should represent both seasonal inorganic–organic partitioning and episodic regional burning, particularly the effects of fire emissions on particle number and size distributions.

Code, data, or code and data availability

All datasets used in this work are published by the ARM User Facility available at https://adc.arm.gov/. In this work, we used the sgpacsmcdceE13.c2 (DOI: 10.5439/1763029, Zawadowicz et al., 2021), sgpaoppsap1flynn1mE13.c1 (DOI: 10.5439/1369240, Koontz et al., 2021), sgpaossmpsE13.b1 (DOI: 10.5439/1476898, Singh et al., 2021) and sgpaosccn2colaE13.b1 (DOI: 10.5439/1323892, Koontz et al., 2016) data products.

https://doi.org/10.5194/egusphere-2026-3129
Preprint. Discussion started: 27 July 2026

Author contributions

MAZ designed the study, performed the analysis and drafted the manuscript with contributions from all the co-authors. AD provided the LASIC and ORACLES data. JU and RT were responsible for operation of the CCN and optical instruments at SGP during the study period.

Competing interests

The authors declare no competing interests.

Acknowledgements

ARM SGP measurements were obtained from the Atmospheric Radiation Measurement (ARM) Program sponsored by the U.S. Department of Energy, Office of Science, Office of Biological and Environmental Research, Climate and Environmental Sciences Division. This research was supported by the Office of Biological and Environmental Research (BER) Atmospheric Research Program (ASR) in the Department of Energy, Office of Science, and through the U.S. Department of Energy Contract DE-SC0012704 to Brookhaven National Laboratory.

References

Andreae, M. O. and Rosenfeld, D.: Aerosol–cloud–precipitation interactions. Part 1. The nature and sources of cloud-active aerosols, Earth-Science Reviews, 89, 13–41, https://doi.org/10.1016/j.earscirev.2008.03.001, 2008.

Canonaco, F., Crippa, M., Slowik, J. G., Baltensperger, U., and Prévôt, A. S. H.: SoFi, an IGOR-based interface for the efficient use of the generalized multilinear engine (ME-2) for the source apportionment: ME-2 application to aerosol mass spectrometer data, Atmos. Meas. Tech., 6, 3649–3661, https://doi.org/10.5194/amt-6-3649-2013, 2013.

Canonaco, F., Tobler, A., Chen, G., Sosedova, Y., Slowik, J. G., Bozzetti, C., Daellenbach, K. R., El Haddad, I., Crippa, M., Huang, R.-J., Furger, M., Baltensperger, U., and Prévôt, A. S. H.: A new method for long-term source apportionment with time-dependent factor profiles and uncertainty assessment using SoFi Pro: application to 1 year of organic aerosol data, Atmos. Meas. Tech., 14, 923–943, https://doi.org/10.5194/amt-14-923-2021, 2021a.

Canonaco, F., Tobler, A., Chen, G., Sosedova, Y., Slowik, J. G., Bozzetti, C., Daellenbach, K. R., El Haddad, I., Crippa, M., Huang, R.-J., Furger, M., Baltensperger, U., and Prévôt, A. S. H.: A new method for long-term source apportionment with time-dependent factor profiles and uncertainty assessment using SoFi Pro: application to 1 year of organic aerosol data, Atmos. Meas. Tech., 14, 923–943, https://doi.org/10.5194/amt-14-923-2021, 2021b.

Crippa, M., Canonaco, F., Lanz, V. A., Äijälä, M., Allan, J. D., Carbone, S., Capes, G., Ceburnis, D., Dall'Osto, M., Day, D. A., DeCarlo, P. F., Ehn, M., Eriksson, A., Freney, E., Hildebrandt Ruiz, L., Hillamo, R., Jimenez, J. L., Junninen, H., Kiendler-Scharr, A., Kortelainen, A.-M., Kulmala, M., Laaksonen, A., Mensah, A. A., Mohr, C., Nemitz, E., O'Dowd, C., Ovadnevaite, J., Pandis, S. N., Petäjä, T., Poulain, L., Saarikoski, S., Sellegri, K., Swietlicki, E., Tiitta, P., Worsnop, D. R., Baltensperger,

https://doi.org/10.5194/egusphere-2026-3129
Preprint. Discussion started: 27 July 2026

U., and Prévôt, A. S. H.: Organic aerosol components derived from 25 AMS data sets across Europe using a consistent ME-2 based source apportionment approach, Atmos. Chem. Phys., 14, 6159–6176, https://doi.org/10.5194/acp-14-6159-2014, 2014.

Cubison, M. J., Ortega, A. M., Hayes, P. L., Farmer, D. K., Day, D., Lechner, M. J., Brune, W. H., Apel, E., Diskin, G. S., Fisher, J. A., Fuelberg, H. E., Hecobian, A., Knapp, D. J., Mikoviny, T., Riemer, D., Sachse, G. W., Sessions, W., Weber, R. J., Weinheimer, A. J., Wisthaler, A., and Jimenez, J. L.: Effects of aging on organic aerosol from open biomass burning smoke in aircraft and laboratory studies, Atmos. Chem. Phys., 11, 12049–12064, https://doi.org/10.5194/acp-11-12049-2011, 2011.

Dobracki, A., Zuidema, P., Howell, S. G., Saide, P., Freitag, S., Aiken, A. C., Burton, S. P., Sedlacek Iii, A. J., Redemann, J., and Wood, R.: An attribution of the low single-scattering albedo of biomass burning aerosol over the southeastern Atlantic, Atmos. Chem. Phys., 23, 4775–4799, https://doi.org/10.5194/acp-23-4775-2023, 2023.

Dobracki, A., Lewis, E. R., Sedlacek Iii, A. J., Tatro, T., Zawadowicz, M. A., and Zuidema, P.: Burning conditions and transportation pathways determine biomass-burning aerosol properties in the Ascension Island marine boundary layer, Atmos. Chem. Phys., 25, 2333–2363, https://doi.org/10.5194/acp-25-2333-2025, 2025.

Fleming, Z. L., Monks, P. S., and Manning, A. J.: Review: Untangling the influence of air-mass history in interpreting observed atmospheric composition, Atmospheric Research, 104–105, 1–39, https://doi.org/10.1016/j.atmosres.2011.09.009, 2012.

Flynn, C., Ermold, B., Chand, D., and Koontz, A.: The ARM Aerosol Optical Properties (AOP) Value-Added Product, Atmospheric Radiation Measurement, 2020.

Fountoukis, C. and Nenes, A.: ISORROPIA II: a computationally efficient thermodynamic equilibrium model for K^+ –Ca^{2+} –Mg^{2+} –NH_4^+ –Na^+ –SO_4^{2-} –NO_3^- –Cl^- –H_2O aerosols, Atmos. Chem. Phys., 7, 4639–4659, https://doi.org/10.5194/acp-7-4639-2007, 2007.

Guenther, A. B., Jiang, X., Heald, C. L., Sakulyanontvittaya, T., Duhl, T., Emmons, L. K., and Wang, X.: The Model of Emissions of Gases and Aerosols from Nature version 2.1 (MEGAN2.1): an extended and updated framework for modeling biogenic emissions, Geosci. Model Dev., 5, 1471–1492, https://doi.org/10.5194/gmd-5-1471-2012, 2012.

Hand, J. L.: IMPROVE Data User Guide 2023 (Version 2), 2023.

Hand, J. L., Gebhart, K. A., Schichtel, B. A., and Malm, W. C.: Increasing trends in wintertime particulate sulfate and nitrate ion concentrations in the Great Plains of the United States (2000–2010), Atmospheric Environment, 55, 107–110, https://doi.org/10.1016/j.atmosenv.2012.03.050, 2012.

Heikkinen, L., Äijälä, M., Riva, M., Luoma, K., Dällenbach, K., Aalto, J., Aalto, P., Aliaga, D., Aurela, M., Keskinen, H., Makkonen, U., Rantala, P., Kulmala, M., Petäjä, T., Worsnop, D., and Ehn, M.: Long-term sub-micrometer aerosol chemical composition in the boreal forest: inter- and intra-annual variability, Atmos. Chem. Phys., 20, 3151–3180, https://doi.org/10.5194/acp-20-3151-2020, 2020.

Hennigan, C. J., Sullivan, A. P., Collett, J. L., and Robinson, A. L.: Levoglucosan stability in biomass burning particles exposed to hydroxyl radicals, Geophysical Research Letters, 37, 2010GL043088, https://doi.org/10.1029/2010GL043088, 2010.

Henry, R., Norris, G. A., Vedantham, R., and Turner, J. R.: Source region identification using kernel smoothing, Environ. Sci. Technol., 43, 4090–4097, https://doi.org/10.1021/es8011723, 2009.

Hermann, M., Wehner, B., Bischof, O., Han, H.-S., Krinke, T., Liu, W., Zerrath, A., and Wiedensohler, A.: Particle counting efficiencies of new TSI condensation particle counters, Journal of Aerosol Science, 38, 674–682, https://doi.org/10.1016/j.jaerosci.2007.05.001, 2007.

https://doi.org/10.5194/egusphere-2026-3129
Preprint. Discussion started: 27 July 2026

Hidy, G. M., Blanchard, C. L., Baumann, K., Edgerton, E., Tanenbaum, S., Shaw, S., Knipping, E., Tombach, I., Jansen, J., and Walters, J.: Chemical climatology of the southeastern United States, 1999–2013, Atmos. Chem. Phys., 14, 11893–11914, https://doi.org/10.5194/acp-14-11893-2014, 2014.

Hodshire, A. L., Bian, Q., Ramnarine, E., Lonsdale, C. R., Alvarado, M. J., Kreidenweis, S. M., Jathar, S. H., and Pierce, J. R.: More Than Emissions and Chemistry: Fire Size, Dilution, and Background Aerosol Also Greatly Influence Near-Field Biomass Burning Aerosol Aging, JGR Atmospheres, 124, 5589–5611, https://doi.org/10.1029/2018JD029674, 2019.

Jacob, D. J., Crawford, J. H., Maring, H., Clarke, A. D., Dibb, J. E., Emmons, L. K., Ferrare, R. A., Hostetler, C. A., Russell, P. B., Singh, H. B., Thompson, A. M., Shaw, G. E., McCauley, E., Pederson, J. R., and Fisher, J. A.: The Arctic Research of the Composition of the Troposphere from Aircraft and Satellites (ARCTAS) mission: design, execution, and first results, Atmos. Chem. Phys., 10, 5191–5212, https://doi.org/10.5194/acp-10-5191-2010, 2010.

Jimenez, J. L., Canagaratna, M. R., Donahue, N. M., Prevot, A. S. H., Zhang, Q., Kroll, J. H., DeCarlo, P. F., Allan, J. D., Coe, H., Ng, N. L., Aiken, A. C., Docherty, K. S., Ulbrich, I. M., Grieshop, A. P., Robinson, A. L., Duplissy, J., Smith, J. D., Wilson, K. R., Lanz, V. A., Hueglin, C., Sun, Y. L., Tian, J., Laaksonen, A., Raatikainen, T., Rautiainen, J., Vaattovaara, P., Ehn, M., Kulmala, M., Tomlinson, J. M., Collins, D. R., Cubison, M. J., E., Dunlea, J., Huffman, J. A., Onasch, T. B., Alfarra, M. R., Williams, P. I., Bower, K., Kondo, Y., Schneider, J., Drewnick, F., Borrmann, S., Weimer, S., Demerjian, K., Salcedo, D., Cottrell, L., Griffin, R., Takami, A., Miyoshi, T., Hatakeyama, S., Shimono, A., Sun, J. Y., Zhang, Y. M., Dzepina, K., Kimmel, J. R., Sueper, D., Jayne, J. T., Herndon, S. C., Trimborn, A. M., Williams, L. R., Wood, E. C., Middlebrook, A. M., Kolb, C. E., Baltensperger, U., and Worsnop, D. R.: Evolution of Organic Aerosols in the Atmosphere, Science, 326, 1525–1529, https://doi.org/10.1126/science.1180353, 2009.

Kaiser, J. W., Heil, A., Andreae, M. O., Benedetti, A., Chubarova, N., Jones, L., Morcrette, J.-J., Razinger, M., Schultz, M. G., Suttie, M., and Van Der Werf, G. R.: Biomass burning emissions estimated with a global fire assimilation system based on observed fire radiative power, Biogeosciences, 9, 527–554, https://doi.org/10.5194/bg-9-527-2012, 2012.

Kim, P. S., Jacob, D. J., Fisher, J. A., Travis, K., Yu, K., Zhu, L., Yantosca, R. M., Sulprizio, M. P., Jimenez, J. L., Campuzano-Jost, P., Froyd, K. D., Liao, J., Hair, J. W., Fenn, M. A., Butler, C. F., Wagner, N. L., Gordon, T. D., Welti, A., Wennberg, P. O., Crounse, J. D., St. Clair, J. M., Teng, A. P., Millet, D. B., Schwarz, J. P., Markovic, M. Z., and Perring, A. E.: Sources, seasonality, and trends of southeast US aerosol: an integrated analysis of surface, aircraft, and satellite observations with the GEOS-Chem chemical transport model, Atmos. Chem. Phys., 15, 10411–10433, https://doi.org/10.5194/acp-15-10411-2015, 2015.

Kim, Y. J., Spak, S. N., Carmichael, G. R., Riemer, N., and Stanier, C. O.: Modeled aerosol nitrate formation pathways during wintertime in the Great Lakes region of North America, JGR Atmospheres, 119, https://doi.org/10.1002/2014JD022320, 2014.

Koontz, A., Uin, J., Andrews, E., Enekwizu, O., Hayes, C., and Salwen, C.: aosccn2cola.b1, https://doi.org/10.5439/1323892, 2016.

Koontz, A., Flynn, C., and Shilling, J.: aoppsap1flynn1m.c1, https://doi.org/10.5439/1369240, 2021.

Malm, W. C. and Hand, J. L.: An examination of the physical and optical properties of aerosols collected in the IMPROVE program, Atmospheric Environment, 41, 3407–3427, https://doi.org/10.1016/j.atmosenv.2006.12.012, 2007.

Malm, W. C., Sisler, J. F., Huffman, D., Eldred, R. A., and Cahill, T. A.: Spatial and seasonal trends in particle concentration and optical extinction in the United States, J. Geophys. Res., 99, 1347–1370, https://doi.org/10.1029/93JD02916, 1994.

Marais, E. A., Jacob, D. J., Jimenez, J. L., Campuzano-Jost, P., Day, D. A., Hu, W., Krechmer, J., Zhu, L., Kim, P. S., Miller, C. C., Fisher, J. A., Travis, K., Yu, K., Hanisco, T. F., Wolfe, G. M., Arkinson, H. L., Pye, H. O. T., Froyd, K. D., Liao, J.,

https://doi.org/10.5194/egusphere-2026-3129
Preprint. Discussion started: 27 July 2026

and McNeill, V. F.: Aqueous-phase mechanism for secondary organic aerosol formation from isoprene: application to the southeast United States and co-benefit of SO_2 emission controls, Atmos. Chem. Phys., 16, 1603–1618, https://doi.org/10.5194/acp-16-1603-2016, 2016.

May, A. A., Saleh, R., Hennigan, C. J., Donahue, N. M., and Robinson, A. L.: Volatility of Organic Molecular Markers Used for Source Apportionment Analysis: Measurements and Implications for Atmospheric Lifetime, Environ. Sci. Technol., 46, 12435–12444, https://doi.org/10.1021/es302276t, 2012.

McComiskey, A. and Ferrare, R. A.: Aerosol Physical and Optical Properties and Processes in the ARM Program, Meteorological Monographs, 57, 21.1-21.17, https://doi.org/10.1175/AMSMONOGRAPHS-D-15-0028.1, 2016.

Ng, N. L., Canagaratna, M. R., Zhang, Q., Jimenez, J. L., Tian, J., Ulbrich, I. M., Kroll, J. H., Docherty, K. S., Chhabra, P. S., Bahreini, R., Murphy, S. M., Seinfeld, J. H., Hildebrandt, L., Donahue, N. M., DeCarlo, P. F., Lanz, V. A., Prévôt, A. S. H., Dinar, E., Rudich, Y., and Worsnop, D. R.: Organic aerosol components observed in Northern Hemispheric datasets from Aerosol Mass Spectrometry, Atmos. Chem. Phys., 10, 4625–4641, https://doi.org/10.5194/acp-10-4625-2010, 2010.

Ng, N. L., Herndon, S. C., Trimborn, A., Canagaratna, M. R., Croteau, P. L., Onasch, T. B., Sueper, D., Worsnop, D. R., Zhang, Q., Sun, Y. L., and Jayne, J. T.: An Aerosol Chemical Speciation Monitor (ACSM) for Routine Monitoring of the Composition and Mass Concentrations of Ambient Aerosol, Aerosol Science and Technology, 45, 780–794, https://doi.org/10.1080/02786826.2011.560211, 2011.

NOAA National Centers for Environmental Information: Monthly Wildfires Report for Annual 2023, NOAA National Centers for Environmental Information, 2024.

Ortega, A. M., Day, D. A., Cubison, M. J., Brune, W. H., Bon, D., De Gouw, J. A., and Jimenez, J. L.: Secondary organic aerosol formation and primary organic aerosol oxidation from biomass-burning smoke in a flow reactor during FLAME-3, Atmos. Chem. Phys., 13, 11551–11571, https://doi.org/10.5194/acp-13-11551-2013, 2013.

Paatero, P.: The multilinear engine: a table-driven, least squares program for solving multilinear problems, including the n-Way parallel factor analysis model, Journal of Computational and Graphical Statistics, 8, 854, https://doi.org/10.2307/1390831, 1999.

Paatero, P. and Tapper, U.: Positive matrix factorization: A non-negative factor model with optimal utilization of error estimates of data values, Environmetrics, 5, 111–126, https://doi.org/10.1002/env.3170050203, 1994.

Parworth, C., Fast, J., Mei, F., Shippert, T., Sivaraman, C., Tilp, A., Watson, T., and Zhang, Q.: Long-term measurements of submicrometer aerosol chemistry at the Southern Great Plains (SGP) using an Aerosol Chemical Speciation Monitor (ACSM), Atmospheric Environment, 106, 43–55, https://doi.org/10.1016/j.atmosenv.2015.01.060, 2015.

Petit, J.-E., Favez, O., Albinet, A., and Canonaco, F.: A user-friendly tool for comprehensive evaluation of the geographical origins of atmospheric pollution: Wind and trajectory analyses, Environmental Modelling & Software, 88, 183–187, https://doi.org/10.1016/j.envsoft.2016.11.022, 2017.

Prospero, J. M., Barkley, A. E., Gaston, C. J., Gatineau, A., Campos Y Sansano, A., and Panechou, K.: Characterizing and Quantifying African Dust Transport and Deposition to South America: Implications for the Phosphorus Budget in the Amazon Basin, Global Biogeochemical Cycles, 34, e2020GB006536, https://doi.org/10.1029/2020GB006536, 2020.

Schmale, J., Henning, S., Decesari, S., Henzing, B., Keskinen, H., Sellegri, K., Ovadnevaite, J., Pöhlker, M. L., Brito, J., Bougiatioti, A., Kristensson, A., Kalivitis, N., Stavroulas, I., Carbone, S., Jefferson, A., Park, M., Schlag, P., Iwamoto, Y., Aalto, P., Äijälä, M., Bukowiecki, N., Ehn, M., Frank, G., Fröhlich, R., Frumau, A., Herrmann, E., Herrmann, H., Holzinger,

https://doi.org/10.5194/egusphere-2026-3129
Preprint. Discussion started: 27 July 2026

R., Kos, G., Kulmala, M., Mihalopoulos, N., Nenes, A., O'Dowd, C., Petäjä, T., Picard, D., Pöhlker, C., Pöschl, U., Poulain, L., Prévôt, A. S. H., Swietlicki, E., Andreae, M. O., Artaxo, P., Wiedensohler, A., Ogren, J., Matsuki, A., Yum, S. S., Stratmann, F., Baltensperger, U., and Gysel, M.: Long-term cloud condensation nuclei number concentration, particle number size distribution and chemical composition measurements at regionally representative observatories, Atmos. Chem. Phys., 18, 2853–2881, https://doi.org/10.5194/acp-18-2853-2018, 2018.

Schulze, B. C., Wallace, H. W., Bui, A. T., Flynn, J. H., Erickson, M. H., Alvarez, S., Dai, Q., Usenko, S., Sheesley, R. J., and Griffin, R. J.: The impacts of regional shipping emissions on the chemical characteristics of coastal submicron aerosols near Houston, TX, Atmos. Chem. Phys., 18, 14217–14241, https://doi.org/10.5194/acp-18-14217-2018, 2018.

Sedlacek, A. J., Lewis, E. R., Onasch, T. B., Zuidema, P., Redemann, J., Jaffe, D., and Kleinman, L. I.: Using the Black Carbon Particle Mixing State to Characterize the Lifecycle of Biomass Burning Aerosols, Environ. Sci. Technol., 56, 14315–14325, https://doi.org/10.1021/acs.est.2c03851, 2022.

Shrivastava, M., Cappa, C. D., Fan, J., Goldstein, A. H., Guenther, A. B., Jimenez, J. L., Kuang, C., Laskin, A., Martin, S. T., Ng, N. L., Petaja, T., Pierce, J. R., Rasch, P. J., Roldin, P., Seinfeld, J. H., Shilling, J., Smith, J. N., Thornton, J. A., Volkamer, R., Wang, J., Worsnop, D. R., Zaveri, R. A., Zelenyuk, A., and Zhang, Q.: Recent advances in understanding secondary organic aerosol: Implications for global climate forcing, Reviews of Geophysics, 55, 509–559, https://doi.org/10.1002/2016RG000540, 2017.

Singh, A., Kuang, C., Howie, J., Salwen, C., and Hayes, C.: Scanning Mobility Particle Sizer, b1 level, https://doi.org/10.5439/1476898, 2021.

Sisterson, D. L., Peppler, R. A., Cress, T. S., Lamb, P. J., and Turner, D. D.: The ARM Southern Great Plains (SGP) Site, Meteorological Monographs, 57, 6.1-6.14, https://doi.org/10.1175/AMSMONOGRAPHS-D-16-0004.1, 2016.

Stanier, C., Singh, A., Adamski, W., Baek, J., Caughey, M., Carmichael, G., Edgerton, E., Kenski, D., Koerber, M., Oleson, J., Rohlf, T., Lee, S. R., Riemer, N., Shaw, S., Sousan, S., and Spak, S. N.: Overview of the LADCO winter nitrate study: hourly ammonia, nitric acid and $PM_{2.5}$ composition at an urban and rural site pair during $PM_{2.5}$ episodes in the US Great Lakes region, Atmos. Chem. Phys., 12, 11037–11056, https://doi.org/10.5194/acp-12-11037-2012, 2012.

Stein, A. F., Draxler, R. R., Rolph, G. D., Stunder, B. J. B., Cohen, M. D., and Ngan, F.: NOAA's HYSPLIT Atmospheric Transport and Dispersion Modeling System, Bulletin of the American Meteorological Society, 96, 2059–2077, https://doi.org/10.1175/BAMS-D-14-00110.1, 2015.

Subramanian, R., Khlystov, A. Y., Cabada, J. C., and Robinson, A. L.: Positive and Negative Artifacts in Particulate Organic Carbon Measurements with Denuded and Undenuded Sampler Configurations Special Issue of *Aerosol Science and Technology* on Findings from the Fine Particulate Matter Supersites Program, Aerosol Science and Technology, 38, 27–48, https://doi.org/10.1080/02786820390229354, 2004.

Thompson, S. A., Chen, B., Matthews, B. H., Li, R., Nowotarski, C. J., Rapp, A. D., and Brooks, S. D.: Characterizing Greater Houston's Aerosol by Air Mass During TRACER, JGR Atmospheres, 130, e2025JD043353, https://doi.org/10.1029/2025JD043353, 2025.

Turpin, B. J., Huntzicker, J. J., and Hering, S. V.: Investigation of organic aerosol sampling artifacts in the los angeles basin, Atmospheric Environment, 28, 3061–3071, https://doi.org/10.1016/1352-2310(94)00133-6, 1994.

Twohy, C. H., Toohey, D. W., Levin, E. J. T., DeMott, P. J., Rainwater, B., Garofalo, L. A., Pothier, M. A., Farmer, D. K., Kreidenweis, S. M., Pokhrel, R. P., Murphy, S. M., Reeves, J. M., Moore, K. A., and Fischer, E. V.: Biomass Burning Smoke

https://doi.org/10.5194/egusphere-2026-3129
Preprint. Discussion started: 27 July 2026

and Its Influence on Clouds Over the Western U. S., Geophysical Research Letters, 48, e2021GL094224, https://doi.org/10.1029/2021GL094224, 2021.

Uin, J., Aiken, A. C., Dubey, M. K., Kuang, C., Pekour, M., Salwen, C., Sedlacek, A. J., Senum, G., Smith, S., Wang, J., Watson, T. B., and Springston, S. R.: Atmospheric Radiation Measurement (ARM) Aerosol Observing Systems (AOS) for Surface-Based In Situ Atmospheric Aerosol and Trace Gas Measurements, Journal of Atmospheric and Oceanic Technology, 36, 2429–2447, https://doi.org/10.1175/JTECH-D-19-0077.1, 2019.

Ulbrich, I. M., Canagaratna, M. R., Zhang, Q., Worsnop, D. R., and Jimenez, J. L.: Interpretation of organic components from Positive Matrix Factorization of aerosol mass spectrometric data, Atmos. Chem. Phys., 9, 2891–2918, https://doi.org/10.5194/acp-9-2891-2009, 2009.

Zawadowicz, M., Howie, J., Shilling, J., and Levin, M.: Aerosol Chemical Speciation Monitor, mentor processed, .c2, https://doi.org/10.5439/1763029, 2021.

Zhang, Q., Jimenez, J. L., Canagaratna, M. R., Allan, J. D., Coe, H., Ulbrich, I., Alfarra, M. R., Takami, A., Middlebrook, A. M., Sun, Y. L., Dzepina, K., Dunlea, E., Docherty, K., DeCarlo, P. F., Salcedo, D., Onasch, T., Jayne, J. T., Miyoshi, T., Shimono, A., Hatakeyama, S., Takegawa, N., Kondo, Y., Schneider, J., Drewnick, F., Borrmann, S., Weimer, S., Demerjian, K., Williams, P., Bower, K., Bahreini, R., Cottrell, L., Griffin, R. J., Rautiainen, J., Sun, J. Y., Zhang, Y. M., and Worsnop, D. R.: Ubiquity and dominance of oxygenated species in organic aerosols in anthropogenically-influenced Northern Hemisphere midlatitudes, Geophysical Research Letters, 34, 2007GL029979, https://doi.org/10.1029/2007GL029979, 2007.

Zhang, Q., Jimenez, J. L., Canagaratna, M. R., Ulbrich, I. M., Ng, N. L., Worsnop, D. R., and Sun, Y.: Understanding atmospheric organic aerosols via factor analysis of aerosol mass spectrometry: a review, Anal Bioanal Chem, 401, 3045–3067, https://doi.org/10.1007/s00216-011-5355-y, 2011.